Collective Coordinates Theory for Discrete Soliton Ratchets in the sine-Gordon Model

Bernardo Sánchez-Rey*
Departamento de Física Aplicada I, E.P.S., Universidad de Sevilla, Virgen de África 7, 41011, Sevilla, Spain

Niurka R. Quintero† and J. Cuevas-Maraver‡
Instituto de Matemáticas de la Universidad de Sevilla (IMUS) and
Departamento de Física Aplicada I, E.P.S., Universidad de Sevilla, Virgen de África 7, 41011, Sevilla, Spain

Miguel A. Alejo§
Instituto Nacional de Matemática Pura e Aplicada (IMPA),
Estrada Dona Castorina 110, 22460-320, Rio de Janeiro, Brazil
(Dated: July 1, 2014)

A collective coordinate theory is develop for soliton ratchets in the damped discrete sine-Gordon model driven by a biharmonic force. An *ansatz* with two collective coordinates, namely the center and the width of the soliton, is assumed as an approximated solution of the discrete non-linear equation. The evolution of these two collective coordinates, obtained by means of the Generalized Travelling Wave Method, explains the mechanism underlying the soliton ratchet and captures qualitatively all the main features of this phenomenon. The theory accounts for the existence of a non-zero depinning threshold, the non-sinusoidal behaviour of the average velocity as a function of the difference phase between the harmonics of the driver, the non-monotonic dependence of the average velocity on the damping and the existence of non-transporting regimes beyond the depinning threshold. In particular it provides a good description of the intriguing and complex pattern of subspaces corresponding to different dynamical regimes in parameter space.

PACS numbers: 05.45Yv, 63.20Ry
Keywords: Soliton ratchet, sine-Gordon equation, collective coordinates, Generalized Travelling Wave Method, depinning.

arXiv:1406.7656v1 [nlin.PS] 30 Jun 2014

I. INTRODUCTION

Soliton Ratchet [1–3] is a generalization of the ratchet effect [4] to spatially extended systems described by nonlinear partial differential equations (PDE). In these systems, nonlinear coherent excitations play a key role for transport properties and the ratchet effect appears as a directed motion of solitons under the influence of zero mean forces, due to the breaking of the spatiotemporal or field symmetries of the system [2, 5, 6].

This phenomenon has been observed experimentally in long Josephson junctions (JJ) devices. In this system, a spatially asymmetric sawtooth ratchet potential can be emulated using a inhomogeneous magnetic field [7], giving rise to drift dynamics of fluxons (magnetic flux quanta) similar to that observed for particle-point ratchets. The break of the spatial symmetry can also be achieved by properly injecting an external current [8] or by introducing a modulation of the coupling between junctions [9, 10]. Another means to obtain a fluxon ratchet is that of breaking the temporal symmetry. That was performed in an annular JJ using a bi-harmonic force accomplished with microwaves [11].

The mechanism underlying soliton ratchets in continuous systems has been clarified in detail by a collective coordinates (CC) theory [5, 12–15]. In this theory, the center of mass, $X(t)$, and the width, $l(t)$, of the soliton are independent dynamical variables and the initial PDE is reduced to a pair of coupled nonlinear ordinary differential equations (ODE) for the two CCs. Net soliton motion becomes possible when the indirect driving resonates with one of the available frequencies of the soliton internal vibrations. If this resonant condition is fulfilled, the energy pumped by the driver into the soliton internal vibration is converted into net motion through its coupling with the translational degree of freedom.

Soliton ratchets have also been investigated in discrete systems [16–20]. In contrast with the continuous case, the interplay between discreteness and nonlinearity introduces new features such as: non-zero depinning threshold [21], staircase dependence of the mean velocity on system parameters, chaotic or intermittent ratchet-like dynamics and the intriguing phenomenon of the existence of non-transporting regimes beyond the depinning threshold [17]. However, most studies are numerical due to the lack of an adequate analytical approximation for strongly discrete systems. The aim of this paper is precisely to address this challenge by developing a two-CC theory that captures all the rich phenomenology of the discrete soliton ratchets in the Frenkel-Kontorova model.

The paper is organized as follows. In Sec. II the damped Frenkel-Kontorova model driven by external bi-harmonic force is introduced. An *ansatz* with two collective coordinates is suggested as an approximated solution of this system, and the ODEs, which govern the evolution of the CCs, are obtained by means of the Generalized Travelling Wave Method (GTWM). Section III is devoted to simulations of the original PDE and their comparison with the numerical simulations of the ODEs for the two CCs. The dependence of the soliton mean velocity on various system parameters is studied in de-

*Electronic address: bernardo@us.es
†Electronic address: niurka@us.es
‡Electronic address: jcuevas@us.es
§Electronic address: malejo@impa.br

tail and particular emphasis is laid on the transition from the very discrete limit to the continuous limit. Section IV summarizes the main conclusions of the paper.

II. MODEL AND COLLECTIVE COORDINATES THEORY

We will focus on the paradigmatic case of the damped discrete sine-Gordon (sG) system [22–24]

$$\ddot{\phi}_n - \kappa\Delta_d\phi_n + \frac{dV(\phi_n)}{d\phi_n} = -\alpha\dot{\phi}_n + F(t), \quad n = 1, 2, ..., N. \tag{1}$$

which can be used, for instance, to describe a parallel array of JJs [25] or to model a circular array of underdamped JJs when F is a constant force [26]. Here, ϕ_n is a scalar field, $\dot{\phi}$ is the derivative with respect to time, $\Delta_d\phi_n \equiv \phi_{n+1} + \phi_{n-1} - 2\phi_n$ is the discrete Laplacian, κ is the coupling constant that measures the discreteness of the lattice, α is the dissipation parameter, $F(t)$ is a time-periodic external driving, and $\frac{dV(\phi_n)}{d\phi_n} = \sin(\phi_n) + \lambda\cos(2\phi_n)$ is the derivative of a spatially-periodic potential, which will be spatially asymmetric in case parameter $\lambda \neq 0$. For $F = 0$ and $\lambda \neq 0$, a mechanical analogue of Eq. (1) in terms of a chain of double pendulum was given in [27]. All these magnitudes and parameters are in dimensionless form.

In this system, net motion of topological nonlinear excitations (kinks or antikinks) can arise when the symmetries of Eq. (1), which relate kink solutions with opposite velocities, are broken. In order to describe the resulting ratchet dynamics, a CC theory is presented based on the idea that perturbations of the system act essentially on the center of mass, $X(t)$, and the width, $l(t)$, of the unperturbed discrete kink. In the same spirit as that of the Rice *ansatz* [28] for the continuous sG equation, the discrete kink is approximated with the *ansatz* [29]

$$\phi_n(t) = 4\arctan\left[\exp(\theta_n)\right], \tag{2}$$

where

$$\theta_n = \frac{\kappa^{-1/2}\, n - X(t)}{l(t)} \tag{3}$$

and equations of motion for the CCs are derived using the so-called GTWM. A more complex *ansatz*, which includes a modulation of the Goldstone mode was used in [29] to study the evolution of a propagating kink in the Frenkel-Kontorova model without perturbations. Since only the case of one kink is to be considered, periodic boundary conditions $\phi_{n+N}(t) = \phi_n(t) + 2\pi$ are also adopted, which correspond, for instance, to a circular array of JJs with only one fluxon [11, 30].

The GTWM was introduced in a general way in Ref. [31] and was successfully applied to study the zero temperature dynamics [31] and thermal diffusion [32] of magnetic vortices in the two-dimensional anisotropic Heisenberg model. Closer to our problem, the GTWM has also been used to explain various phenomena of kink dynamics in continuous φ^4 and sG models [33]. In short, according to the GTWM, given an *ansatz* with M collective coordinates $A_1, A_2, ..., A_M$, the procedure to obtain the evolution equation for each CC, A_j ($j = 1, \cdots, M$), involves three steps: i) insert the *ansatz* in the equation that governs the dynamic of the field ϕ_n; ii) multiply the resulting equation by $\frac{\partial\phi_n}{\partial A_j}$; and iii) integrate over the spatial coordinate (sum over all elements n of the lattice in the discrete case). Thus, applying this prescription, after straightforward but cumbersome algebra, the following equations for $X(t)$ and $l(t)$ are attained:

$$I_4\frac{\ddot{X}}{l} + I_5\frac{\ddot{l}}{l} - (I_3 + 2I_5)\frac{\dot{l}^2}{l^2} - I_1\left(\frac{\dot{X}^2}{l^2} + 1\right) - 2(I_2 + I_4)\frac{\dot{X}\dot{l}}{l^2} = -I_5\alpha\frac{\dot{l}}{l} - I_4\alpha\frac{\dot{X}}{l} - I_6F(t) + \frac{\lambda}{2}I_7 + \left(I_1 + \frac{I_8}{12\kappa l^2}\right)\frac{1}{l^2}, \tag{4}$$

$$I_5\frac{\ddot{X}}{l} + I_{10}\frac{\ddot{l}}{l} - (I_9 + 2I_{10})\frac{\dot{l}^2}{l^2} - I_2\left(\frac{\dot{X}^2}{l^2} + 1\right) - 2(I_3 + I_5)\frac{\dot{X}\dot{l}}{l^2} = -I_{10}\alpha\frac{\dot{l}}{l} - I_5\alpha\frac{\dot{X}}{l} - I_{11}F(t) + \frac{\lambda}{2}I_{12} + \left(I_2 + \frac{I_{13}}{12\kappa l^2}\right)\frac{1}{l^2}, \tag{5}$$

where the terms I_j $(j = 1, ..., 13)$ are functions of $X(t)$ and $l(t)$, that can be defined by the following sums

$$I_1 = \sum_{n=1}^{N}\frac{d\phi_n}{d\theta_n}\sin\phi_n = -4\sum_{n=1}^{N}\frac{\sinh\theta_n}{\cosh^3\theta_n}, \tag{6}$$

$$I_2 = \sum_{n=1}^{N}\frac{d\phi_n}{d\theta_n}\theta_n\sin\phi_n = -4\sum_{n=1}^{N}\theta_n\frac{\sinh\theta_n}{\cosh^3\theta_n}, \tag{7}$$

$$I_3 = \sum_{n=1}^{N}\frac{d\phi_n}{d\theta_n}\frac{d^2\phi_n}{d\theta_n^2}\theta_n^2 = -4\sum_{n=1}^{N}\theta_n^2\frac{\sinh\theta_n}{\cosh^3\theta_n}, \tag{8}$$

$$I_4 = \sum_{n=1}^{N}\left(\frac{d\phi_n}{d\theta_n}\right)^2 = 4\sum_{n=1}^{N}\frac{1}{\cosh^2\theta_n}, \tag{9}$$

$$I_5 = \sum_{n=1}^{N}\left(\frac{d\phi_n}{d\theta_n}\right)^2\theta_n = 4\sum_{n=1}^{N}\frac{\theta_n}{\cosh^2\theta_n}, \tag{10}$$

$$I_6 = \sum_{n=1}^{N} \frac{d\phi_n}{d\theta_n} = 2\sum_{n=1}^{N} \frac{1}{\cosh\theta_n}, \tag{11}$$

$$I_7 = \sum_{n=1}^{N} \frac{d\phi_n}{d\theta_n}\cos 2\phi_n = I_6 - 16\sum_{n=1}^{N} \frac{\sinh^2\theta_n}{\cosh^5\theta_n}, \tag{12}$$

$$I_8 = \sum_{n=1}^{N} \frac{d\phi_n}{d\theta_n}\frac{d^4\phi_n}{d\theta_n^4} = I_1 - 24\sum_{n=1}^{N} \frac{\sinh\theta_n}{\cosh^5\theta_n}, \tag{13}$$

$$I_9 = \sum_{n=1}^{N} \frac{d\phi_n}{d\theta_n}\frac{d^2\phi_n}{d\theta_n^2}\theta_n^3 = -4\sum_{n=1}^{N} \theta_n^3\frac{\sinh\theta_n}{\cosh^3\theta_n}, \tag{14}$$

$$I_{10} = \sum_{n=1}^{N} \Big(\frac{d\phi_n}{d\theta_n}\Big)^2\theta_n^2 = 4\sum_{n=1}^{N} \frac{\theta_n^2}{\cosh^2\theta_n}, \tag{15}$$

$$I_{11} = \sum_{n=1}^{N} \frac{d\phi_n}{d\theta_n}\theta_n = 2\sum_{n=1}^{N} \frac{\theta_n}{\cosh\theta_n}, \tag{16}$$

$$I_{12} = \sum_{n=1}^{N} \frac{d\phi_n}{d\theta_n}\theta_n\cos 2\phi_n = I_{11} - 16\sum_{n=1}^{N} \theta_n\frac{\sinh^2\theta_n}{\cosh^5\theta_n}, \tag{17}$$

$$I_{13} = \sum_{n=1}^{N} \frac{d\phi_n}{d\theta_n}\frac{d^4\phi_n}{d\theta_n^4}\theta_n = I_2 - 24\sum_{n=1}^{N} \theta_n\frac{\sinh\theta_n}{\cosh^5\theta_n}. \tag{18}$$

All these sums are periodic functions of $X(t)$ and, therefore, can be expressed as Fourier series (see Appendix A). Numerically, one can check the fast convergence of the series, being the whole series very accurately approximated by the first harmonic. Moreover, one finds that I_5, I_{11} and I_{12} are much smaller than the other I_j terms (see Fig. 7 in the appendix). By bearing in mind these two additional approximations, the following equations of motion for the CCs are finally obtained:

$$\ddot{X} + \left[J_1(\kappa,l)\frac{\dot{l}^2}{l} - J_2(\kappa,l)\dot{X}^2 - J_3(\kappa,l)\right]\sin(2\pi\sqrt{\kappa}\,X) - \frac{\lambda}{2}J_4(\kappa,l)\cos(2\pi\sqrt{\kappa}\,X) - \frac{\dot{X}\dot{l}}{l} = -\alpha\dot{X} - \frac{\pi}{4}lF(t)\,, \tag{19}$$

$$\ddot{l} - \frac{\dot{l}^2}{2l} + \frac{6}{\pi^2}\frac{\dot{X}^2}{l} + J_5(\kappa,l)\dot{X}\dot{l}\sin(2\pi\sqrt{\kappa}\,X) = -\alpha\dot{l} + J_6(\kappa,l), \tag{20}$$

where

$$J_1(\kappa,l) = \frac{\pi}{4\sinh^3(\pi^2\sqrt{\kappa}\,l)}\Big[2 + 3\pi^4\kappa l^2 + (-2+\pi^4\kappa\,l^2)\cosh(2\pi^2\sqrt{\kappa}\,l)\Big], \tag{21}$$

$$J_2(\kappa,l) = \frac{2\pi^3\kappa l}{\sinh(\pi^2\sqrt{\kappa}\,l)}, \tag{22}$$

$$J_3(\kappa,l) = J_2(\kappa,l)l^2 + \frac{\pi^3(3+12\kappa l^2+2\pi^2\kappa l^2)}{6l\sinh(\pi^2\sqrt{\kappa}\,l)} \tag{23}$$

$$J_4(\kappa,l) = \frac{4\pi^3\kappa l^3(2\pi^2\kappa l^2-1)}{3\cosh(\pi^2\sqrt{\kappa}\,l)}, \tag{24}$$

$$J_5(\kappa,l) = \frac{6\pi\sqrt{\kappa}}{\sinh^3(\pi^2\sqrt{\kappa}\,l)}\Big[3\pi^2\sqrt{\kappa}\,l + \pi^2\sqrt{\kappa}\,l\cosh(2\pi^2\sqrt{\kappa}\,l) - 2\sinh(2\pi^2\sqrt{\kappa}\,l)\Big] \tag{25}$$

$$J_6(\kappa,l) = \frac{3[1+4\kappa l^2(1-l^2)]}{2\pi^2\kappa l^3}. \tag{26}$$

Notice that the validity of the dynamical Eqs. (19) and (20) for the CCs is not restricted to the case of sinusoidal forces.

They are also valid for constant forces or for any generic time-dependent force. Futhermore, in the equation for the kink center of mass (19), one can identify the mechanism responsible for the ratchet phenomenon. Indeed, in the right-handside of that equation, the external force, $F(t)$, appears coupled to the internal degree of freedom of the kink, $l(t)$, giving rise to an effective force $l(t)F(t)$. When $l(t)$ contains at least one of the harmonics of $F(t)$ and the difference of phases between these functions satisfy certain conditions, then the average effective force $\langle l(t)F(t)\rangle \neq 0$ and net kink motion appears.

By taking the limit $\kappa \to \infty$ in Eqs. (19) and (20), one recovers the CC equations in the continuous limit [12]

$$\ddot{X} - \frac{\dot{X}\dot{l}}{l} = -\alpha\dot{X} - \frac{\pi}{4}lF(t)\,, \tag{27}$$

$$2l\ddot{l} - \dot{l}^2 + \frac{12}{\pi^2}\dot{X}^2 = -2\alpha l\dot{l} + \frac{12}{\pi^2}(1-l^2). \tag{28}$$

For a given external force $F(t)$, this two-ODE system can be studied using perturbative expansion [12]. In particular, for a bi-harmonic force of the form

$$F(t) = \epsilon[\cos(\omega t) + \cos(2\omega t + \varphi)], \tag{29}$$

at first order in ϵ and after a transient time, the average velocity is given by

$$\langle v\rangle \equiv \lim_{t\to\infty}\frac{1}{t}\int_0^t \dot{X}(\tau)d\tau$$

$$\simeq \frac{3\pi\epsilon^3}{D}\left[\frac{2\sin(\varphi+\chi+\delta_1)}{\sqrt{\alpha^2\omega^2+(\Omega_R^2-\omega^2)^2}} - \frac{\sin(\varphi+\chi-\delta_2)}{\sqrt{4\alpha^2\omega^2+(\Omega_R^2-4\omega^2)^2}}\right], \tag{30}$$

where $D = 256(\alpha^2+\omega^2)\sqrt{\alpha^2+4\omega^2}$, $\Omega_R^2 = 12/\pi^2$ is the so-called Rice's frequency, $\chi = 2\arctan(\omega/\alpha) - \arctan(2\omega/\alpha)$, and $\delta_m = \arctan\left(\frac{\Omega_R^2 - m^2\omega^2}{m\alpha\omega}\right)$. This expression correctly explains why, in the continuous limit and for small amplitudes ϵ, $\langle v\rangle$ is proportional to ϵ^3, depends sinusoidally on the difference phase φ [34], decreases with the frequency ω, and can exhibit current reversals by properly varying the damping or the frequency.

III. NUMERICAL STUDY

The aim of this section is to check the validity of the CC theory by numerically integrating the system of coupled ODEs (19)-(20) and by comparing the results with direct simulations of the discrete sG lattice equation (1). We will focus on the case of ratchets of discrete kinks driven by the bi-harmonic force (29) of period $T = 2\pi/\omega$. As it is well known, in the damped sine-Gordon equation, this bi-harmonic force breaks the temporal symmetry $F(t) = -F(t+T/2)$ and can be used to induce net kink transport. Consequently, the asymmetry parameter λ will heceforth be taken equal to zero hereafter.

In order to carry out the comparison between the two approaches, we need to determine the center of mass and the width of the sG kink profile, ϕ_n, which map the collective coordinates X and l, respectively. Those variables are defined as:

$$X = \Delta\frac{\sum_n n(\phi_{n+1}-\phi_{n-1})^2}{\sum_n(\phi_{n+1}-\phi_{n-1})^2}, \tag{31}$$

$$l = \Delta\frac{\sqrt{12}}{3}\left[\frac{\sum_n n^2(\phi_{n+1}-\phi_{n-1})^2}{\sum_n(\phi_{n+1}-\phi_{n-1})^2} - X^2\right]^{1/2} \tag{32}$$

where $\Delta = 1/\sqrt{\kappa}$ is the discretization parameter.

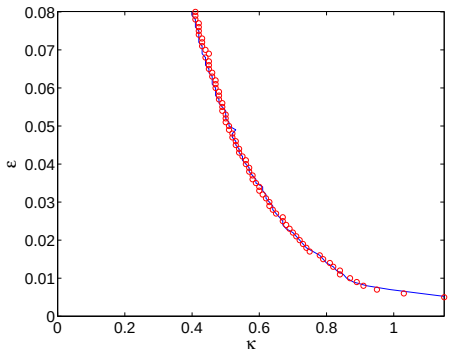

FIG. 1: (Color online) Depinning curve in the plane (κ,ϵ) for $\omega = 0.1$, $\alpha = 0.1$ and $\varphi = 0$. Below the curve no mobile kinks exist. The area above the curve corresponds to moving kinks with nonzero average velocity. The depinning threshold computed from simulation of the discrete sG Eq. (1) (blue solid line) is very well fitted by the results obtained from numerical solutions of the CC equations (red circles).

A first and important test for the CC theory is the estimation of the depinning threshold, i.e., the curve on the (κ,ϵ) plane that separates pinned states from the transporting zone in which moving kinks exist [21]. In Fig. 1 a blue continuous line represents the exact depinning curve obtained from the sG equation (1) for a frequency $\omega = 0.1$. It is computed by starting from a pinned state and increasing ϵ, for a fixed value of κ, until the critical value for which the kink starts to propagate is found. The same numerical experiment with the ODEs for the CCs leads to the red circles, which fit the exact depinning curve very well. As expected, the critical driving amplitude for depinning tends to zero when $\kappa \to \infty$ and the discreteness effects disappear, while in the anticontinuum limit $\kappa \to 0$, the depinning barrier becomes stronger and larger values of ϵ are necessary to overcome this barrier.

Another distinctive feature of kink ratchets in discrete systems that is captured by the CC approximation is the piecewise dependence of the mean velocity on system parameters. For instance, in contrast with the continuous case in which $\langle v\rangle$ has a sinusoidal dependence on the phase difference φ for small amplitudes ϵ, in the discrete case $\langle v\rangle$ becomes zero in intervals whose length increases as the damping is raised [16]. Figure 2(a) shows the dependence of the mean kink velocity on φ for $\kappa = 2$ and $\alpha = 0.1$. Since this lies not far from the continuous limit, the function $\langle v\rangle(\varphi)$ computed from the sG equation (1) (blue continuous line) clearly resembles a sinusoidal function. The results obtained with the CC theory,

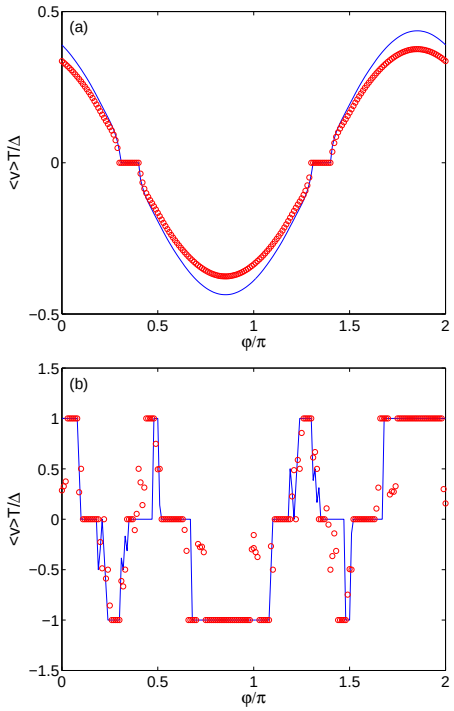

FIG. 2: (Color online) Dependence of the average kink velocity on the phase difference for $\kappa = 2$ (a), and $\kappa = 1$ (b). The blue continuous line represents results obtained from simulations of the sG equation (1). Red circles correspond to results obtained from numerical integration of the CC equations. Other parameters are $\omega = 0.1, \epsilon = 0.05, \alpha = 0.1$.

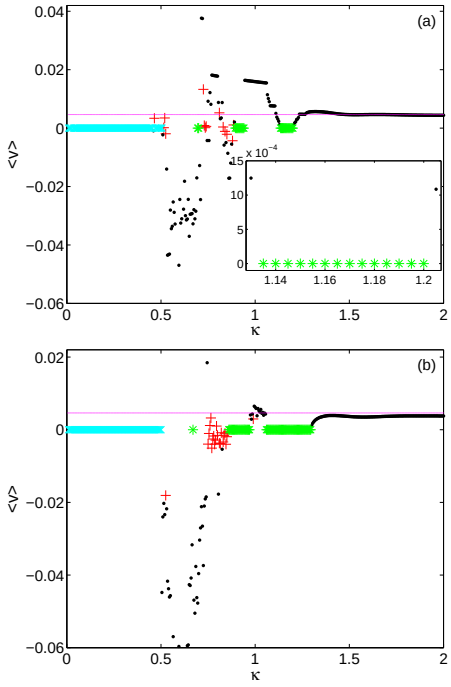

FIG. 3: (Color online) Average kink velocity versus coupling constant. Panels (a) and (b) correspond to the results from simulations of the sG system (1) and from the equations of motion for the CCs (19)-(20), respectively. Symbols refer to different dynamical regimes: periodic or quasiperiodic regular transport (black •), chaotic diffusive transport (red +), pinned states (blue ×) and rotating states (green ∗). Inset shows more detailed behavior around $\kappa = 1.16$. Other parameters: $\omega = 0.1, \epsilon = 0.05, \alpha = 0.1$ and $\varphi = 0$.

plotted with red circles, provide a good approximation and capture the size of the interval without net transport very well.

When κ is decreased, $\langle v \rangle(\varphi)$ loses its resemblance with the sine function and the dependence on φ takes a more complicated shape, as shown in Fig. 2(b) for $\kappa = 1$. One can observe the existence of many pinning intervals, and also the existence of many resonant plateaux at $\langle v \rangle = \pm\Delta/T$, which correspond to kink motion that is perfectly locked to the external driver frequency such that the kink moves exactly one site per driving period. These features could be related with the loss of the regularity of the functional ratchet velocity [35]. The prediction of the CC theory is quantitatively poorer than in Fig. 2(a). This is not surprising because the *ansatz* used is based on the exact solution of the unperturbed system (1) on the continuous limit. But interestingly, the CC approximation provides a reasonable description of what happens when one approaches the very discrete limit.

In Fig.3(a) the transition between the anti-continuous and the continuous limit in the sG system (1) is studied in detail, whereas in Fig.3(b), this transition is considered through solving the CC equations of motion. Remarkably, in spite of the very complex scenario described below, the CC theory captures all the existing dynamical regimes and provides a reasonable qualitative picture of the whole transition. Along the transition path different dynamical regimes appear. For very small κ, below the depinning threshold, the center of the kink remains pinned in a potential well oscillating around its minimum (see blue ×). Above the threshold, regular transport corresponding to periodic (or quasi-periodic) kink trajectories dominates (dots). In this case, after an integer number ℓ of periods T, the kink travels k sites (or very approximately k sites) such that

$$\langle v \rangle = \frac{k\Delta}{\ell T}. \tag{33}$$

Many sudden appearances (and disappearances) of chaotic attractors (red +) leading to diffusive transport are found. The magenta continuous line represents the analytical estimation (30) of the average velocity at the continuous limit. Note that for $\kappa \gtrsim 1.5$, we are already very close to the continuous limit.

Notice also the existence of significative intervals of non-transporting *rotating* states (green asteriks), which are far from the depinning threshold. These correspond to periodic orbits in which the kink center oscillates with an amplitude of typically several sites of the lattice, i.e., during a period T the kink moves k sites forward and afterwards moves backward, coming back exactly to its starting position. The dynamic of this regime is similar to that of a pendulum with *oscillating rotations* (i.e. it rotates k times in one direction, then k times afterwards in the opposite direction, and so forth),

contrary to the pinning states, which resemble a librating pendulum. The dynamics and Fourier spectra of both regimes are compared in Fig. 4. Notice that when the kink is pinned (top panels), then the center of mass oscillates with two harmonics of similar amplitude and the width is almost constant (note the scale on the Y axis). For this reason, the effective force acting on the center of the kink, which is proportional to $l(t)F(t) \approx 1.21F(t)$ has practically zero average. On the other hand, in the rotating regime (bottom panels), the second harmonic of the center of mass has lost weight, width fluctuations are significative (about 5% of the average width) and the second harmonic of the width has gained an importance that was lost by the fourth harmonic. Here, although $l(t)$ oscillates with at least one of the frequencies of the driver $F(t)$ (first resonance condition), the phase difference between these functions is such that $\langle l(t)F(t)\rangle = 0$.

Another significant difference arises when analyzing the Floquet spectrum which enables the spectral stability and internal modes of periodic orbits to be determined. Floquet analysis consists firstly of introducing a perturbation ξ_n to a given solution $\phi_{n,0}$ of the lattice equations (1). The equation for the perturbation therefore reads:

$$\ddot{\xi}_n - \kappa\Delta\xi_n + (\cos\phi_n)\xi_n + \alpha\dot{\xi}_n = 0. \tag{34}$$

The stability properties are given by the spectrum of the Floquet operator $\mathcal{M}$ (whose matrix representation is called *monodromy*) defined as:

$$\begin{pmatrix} \{\xi_n(T)\} \\ \{\dot{\xi}_n(T)\} \end{pmatrix} = \mathcal{M} \begin{pmatrix} \{\xi_n(0)\} \\ \{\dot{\xi}_n(0)\} \end{pmatrix}. \tag{35}$$

The $2N$ monodromy eigenvalues $\Lambda = \exp(\mathrm{i}\theta)$ are dubbed as *Floquet multipliers*, and θ are denoted as *Floquet exponents*. The solution is orbitally stable if all the multipliers lie on or are inside the unit circle. As shown in [36], if Λ is a multiplier, then so are Λ^*, ρ/Λ and ρ/Λ^*, with $\rho = \exp(-\pi\alpha/\omega)$. Consequently, in the absence of bifurcations (in our model, for small κ [21]), all the eigenvalues lie within a circle with radius ρ.

As shown in Ref. [21], pinned states become mobile by means of period-doubling or tangent bifurcations, leading the former to chaotic states and the latter to phase-locked transporting states. Period-doubling (tangent) bifurcations are caused by Floquet multipliers departing at $\Lambda = -1$ ($\Lambda = +1$). In Fig. 5(a), the dependence of the moduli $|\Lambda|$ of the Floquet multipliers are depicted with respect to κ for the pinning states of Fig. 3(a). It is observed that the kink remains stable until $\kappa \approx 0.506$. The transition to a transporting state is mediated by an eigenvalue with exponent $\theta = 0$ that abruptly departs from the circle of radius ρ; that is, the Floquet multipliers stay the whole interval on (or very close to) the ρ-circle. However, in the rotating states, there is always a multiplier with $\theta = 0$ outside the ρ-circle. This is explicitly shown in Fig. 5(b) for the longer interval of rotating states stood out in the inset of Fig. 3(a). Destabilization of the rotating kink at the borders of such an interval gives rise to transporting states with regular dynamics.

An extensive study of the existing dynamical regimes in the parameter (ϵ, κ) plane is displayed in Fig. 6. It is restricted to small values of ϵ because the CC theory fails for $\epsilon > 0.1$. This is in accordance with its perturbative nature and with the fact that, in the discrete sG system, kinks are destroyed above a critical driving by the chaotic dynamics of the whole lattice [16]. Comparison between panels (a) and (b) of Fig. 6 shows that the CC approximation overestimates the green, non-transporting areas but, in general, satisfactorily captures the peculiar and complex pattern in the parameter space.

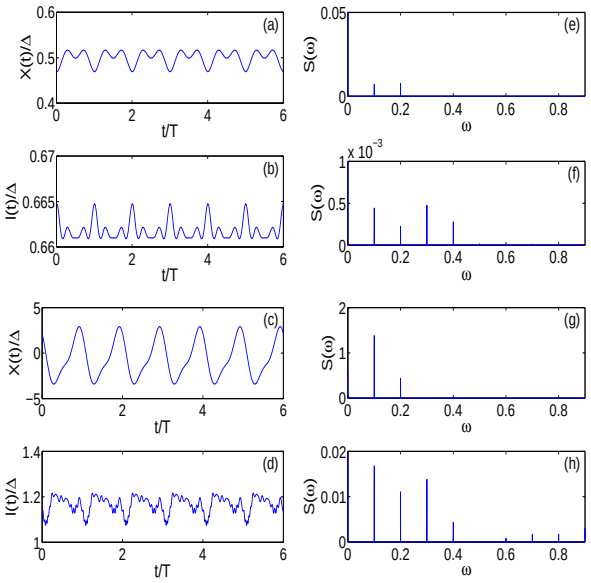

FIG. 4: Evolution of the center of mass and width of the discrete sG kink for $\kappa = 0.3$ (top panels) and $\kappa = 1.2$ (bottom panels). The former case corresponds to a pinning state whereas the latter constitutes an example of a non-transporting rotating state. Fourier spectra for both coordinates are depicted in the right-hand-side panels. Numerical integration of the CC equations (19)-(20) leads to a quantitatively similar outcome. Other parameters are $\omega = 0.1, \epsilon = 0.05, \alpha = 0.1$ and $\varphi = 0$.

Coming back to Fig. 3, another striking aspect is that transport in the discrete system can be very effective. In fact, although in the discrete case kinks have to overcome an energy barrier to move through the lattice (the so-called Peierls-Nabarro barrier), one can observe values in Fig. 3 of the mean kink velocity that are an order of magnitude higher than in the continuous case for the same parameter values. This is actually counter-intuitive. In essence, the Peierls-Nabarro barrier decreases exponentially with κ [23], and therefore one could erroneously expect the kink velocity to be a monotonous increasing function of κ. However, resonance regimes of type (33) can induce very effective transport. Such resonant regimes have also been found in the damped Frenkel-Kontorova model driven by a piecewise constant force [37].

Finally, we have studied the dependence of the kink velocity on the damping. Close to the continuous limit $\langle v\rangle$ displays a characteristic non-monotonic behaviour as shown in Fig. 7(a) for $\kappa = 2$. If $\varphi = 0$, in the underdamped limit, $\langle v\rangle$ vanishes because the discrete sG system (1) becomes invariant under the transformation $t \to -t$ and $\langle v\rangle$ changes its sign.

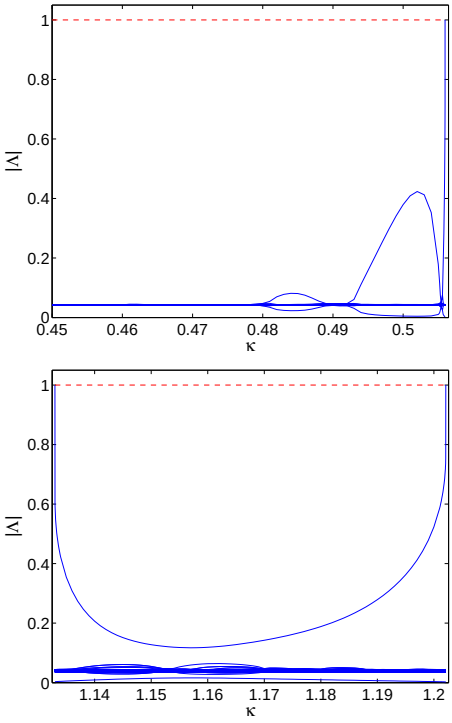

FIG. 5: Top panel: Moduli of Floquet eigenvalues versus coupling constant for the pinning states of Fig. 3(a). Bottom panel: Moduli of Floquet eigenvalues for the rotating states stand out in the inset of Fig. 3(a).

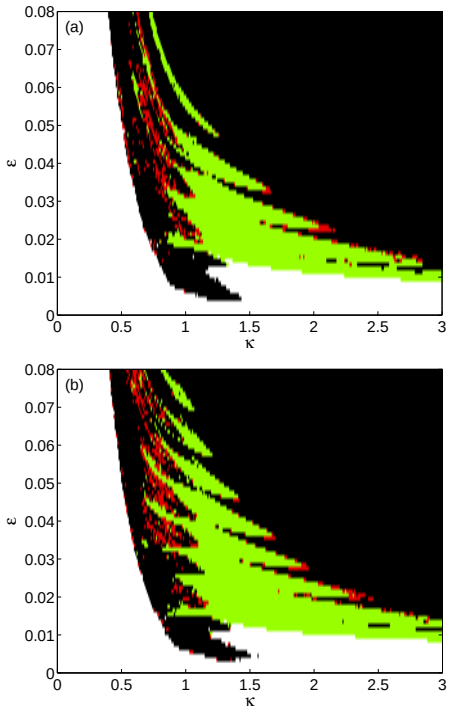

FIG. 6: (Color online) Dynamical regimes of the kink ratchet motion for various values of the coupling constant, κ, and the driving amplitude, ϵ. Panel (a) corresponds to the results from simulations of the discrete sG system (1), and panel (b) to the results from the CC equations of motion. White area: the kink remains pinned; black: periodic or quasiperiodic regular transport; red: chaotic diffusive transport; green: rotating states. Other parameters are $\omega = 0.1$, $\alpha = 0.1$, $\varphi = 0$.

On the other hand, large damping strongly reduces the mobility. As a consequence, transport is maximized for intermediate values of damping [38]. The CC approach (red dashed line) suitable describes this non-monotonous behaviour and the location of the peak.

As the coupling is decreased, kinks lose their mobility quickly and the ratchet effect persists only for small values of damping. For instance, in Fig. 7(b), one can see that for $\kappa = 1$ net transport exists basically for $\alpha \lesssim 0.1$. In that region, $\langle v \rangle$ no longer varies smoothly on α but instead shows the characteristic staircase structure of discrete systems. Although the CC approximation gives the mobility range and the order of magnitude of $\langle v \rangle$ correctly it fails, for small values of damping, in the prediction of a current reversal, which is not observed in the sG system (1).

IV. CONCLUSIONS

We have developed a CC theory for kink ratchets in the damped discrete sine-Gordon equation driven by a bi-harmonic force. Inspired in the Rice *ansatz* used in the continuum sine-Gordon equation [28], a discrete *ansatz* is suggested with two collective coordinates, the center and the width of the soliton, as an approximated solution of our working discrete non-linear equation. The evolution of these two collective coordinates has been obtained by means of the Generalized Travelling Wave Method. The resulting CC theory explains the mechanism underlying the discrete soliton ratchet (the bi-harmonic force with zero average acts on the discrete sG equation, whereas an effective force with, in general, non-zero average acts on the center of kink and causes its motion) and captures the distinctive features of kink motion in discrete systems: namely the existence of a depinning threshold; the piece-wise dependence of the mean velocity on system parameters; and the complicated structure of subspaces of transporting and non-transporting regimes in parameter space.

The numerical study shows that the theory agrees well with the results obtained from simulations of the discrete sG equation close to the continuous limit ($\kappa > 1$) and for small amplitudes of the bi-harmonic force ($\epsilon < 0.1$). This is consistent with the perturbative nature of the CC approach. When $\kappa \leq 1$, the agreement is not good from a quantitative point of view but the CC approximation still provides a reasonable qualitative description of what happens in the very discrete limit.

Particular attention has been devoted to the investigation of the intriguing shape of areas corresponding to different dynamical regimes in phase space. Comparison with exact numerical results of the discrete sG system reveals that the CC approach satisfactorily captures the peculiar and complex structure of subspaces in the parameter plane (ϵ, κ).

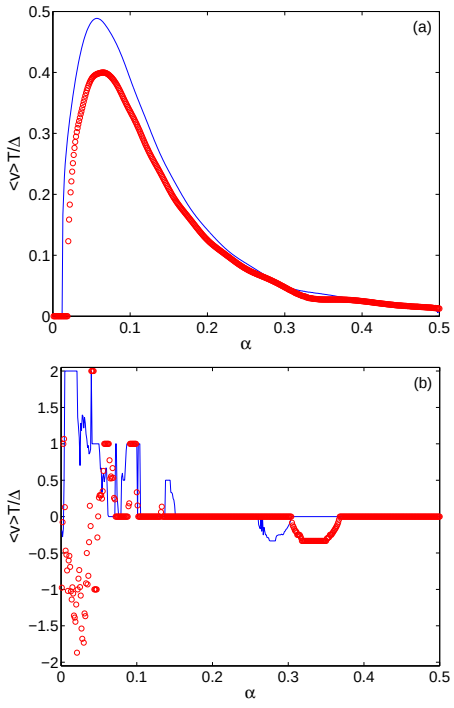

FIG. 7: (Color online) Dependence of the normalized average kink velocity on the damping for $\kappa = 2$ (a), and $\kappa = 1$ (b). The blue solid line represents results from the simulations of the discrete sG equation (1) while the red circles correspond to numerical integration of the CC equations. Other parameters: $\omega = 0.1$, $\epsilon = 0.05$ and $\varphi = 0$.

Further development of the theory is needed in order to extend the method to the case of kink ratchets in asymmetric double sG potentials. In fact, it is easy to verify that the system of CC equations (19)-(20) loses its dependence on the asymmetry parameter, λ, when taking the continuous limit. The challenge is to find an adequate *ansatz* for the asymmetric discrete sG system that leads to a tractable system of ODEs for the CCs.

Appendix A: Approximations for the sums

All the sums I_j $(j = 1, ..., 13)$ defined in the set of equations (6)-(18) are periodic functions of $X(t)$. Therefore, the sums can be expressed as Fourier series and approximated by the first term of each series:

$$I_1 = 16\pi^3\kappa^{3/2}l^3\sum_{n=1}^{\infty}\frac{n^2}{\sinh(n\pi^2\sqrt{\kappa}\,l)}\sin(2n\pi\sqrt{\kappa}X) \approx \frac{16\pi^3\kappa^{3/2}l^3}{\sinh(\pi^2\sqrt{\kappa}\,l)}\sin(2\pi\sqrt{\kappa}\,X), \tag{A1}$$

$$I_2 = -4\sqrt{\kappa}\,l - 16\pi^2\kappa\,l^2\sum_{n=1}^{\infty}\frac{n[1-\frac{n\pi^2\sqrt{\kappa}\,l}{2}\coth(n\pi^2\sqrt{\kappa}\,l)]}{\sinh(n\pi^2\sqrt{\kappa}\,l)}\sin(2n\pi\sqrt{\kappa}X) \approx -4\sqrt{\kappa}\,l, \tag{A2}$$

$$\begin{aligned} I_3 &= \sum_{n=1}^{\infty}\frac{-4\pi\sqrt{\kappa}\,l}{\sinh(n\pi^2\sqrt{\kappa}\,l)}\left[2+n^2\pi^4\kappa\,l^2+2n\pi^2\sqrt{\kappa}\,l\left(-2\coth(n\pi^2\sqrt{\kappa}\,l)+\frac{n\pi^2\sqrt{\kappa}\,l}{\sinh^2(n\pi^2\sqrt{\kappa}\,l)}\right)\right]\sin(2n\pi\sqrt{\kappa}X) \\ &\approx -\frac{4\pi\kappa^{1/2}l}{\sinh(\pi^2\sqrt{\kappa}\,l)}\left[2+\pi^4\kappa l^2-4\pi^2\sqrt{\kappa}\,l\coth(\pi^2\sqrt{\kappa}\,l)+\frac{2\pi^4\kappa l^2}{\sinh^2(\pi^2\sqrt{\kappa}\,l)}\right]\sin(2\pi\sqrt{\kappa}\,X), \end{aligned} \tag{A3}$$

$$I_4 = 8\sqrt{\kappa}\,l + 16\pi^2\kappa l^2\sum_{n=1}^{\infty}\frac{n}{\sinh(n\pi^2\sqrt{\kappa}\,l)}\cos(2n\pi\sqrt{\kappa}X) \approx 8\sqrt{\kappa}\,l, \tag{A4}$$

$$\begin{aligned} I_5 &= 8\pi\sqrt{\kappa}\,l\sum_{n=1}^{\infty}\frac{1-n\pi^2\sqrt{\kappa}\,l\coth(n\pi^2\sqrt{\kappa}\,l)}{\sinh(n\pi^2\sqrt{\kappa}\,l)}\sin(2n\pi\sqrt{\kappa}X) \\ &\approx \frac{8\pi\kappa^{1/2}l[1-\pi^2\sqrt{\kappa}\,l\coth(\pi^2\sqrt{\kappa}\,l)]}{\sinh(\pi^2\sqrt{\kappa}\,l)}\sin(2\pi\sqrt{\kappa}\,X), \end{aligned} \tag{A5}$$

$$I_6 = 2\pi\sqrt{\kappa}\,l + 4\pi\sqrt{\kappa}\,l\sum_{n=1}^{\infty}\frac{\cos(2n\pi\sqrt{\kappa}X)}{\cosh(n\pi^2\sqrt{\kappa}\,l)} \approx 2\pi\sqrt{\kappa}\,l, \tag{A6}$$

$$\begin{aligned} I_7 &= I_6 - 2\pi\sqrt{\kappa}\,l - \frac{4}{3}\pi\sqrt{\kappa}\,l\sum_{n=1}^{\infty}\frac{3+8n^2\pi^2\kappa\,l^2-16n^4\pi^4\kappa^2\,l^4}{\cosh(n\pi^2\sqrt{\kappa}\,l)}\cos(2n\pi\sqrt{\kappa}X) \\ &\approx \frac{32\pi^3\kappa^{3/2}l^3(2\pi^2\kappa l^2-1)}{3\cosh(\pi^2\sqrt{\kappa}\,l)}\cos(2\pi\sqrt{\kappa}\,X), \end{aligned} \tag{A7}$$

$$I_8 = I_1 + 32\sum_{n=1}^{\infty}\frac{n^2\pi^3\kappa^{3/2}\,l^3(1+n^2\pi^2\kappa\,l^2)}{\sinh(n\pi^2\sqrt{\kappa}\,l)}\sin(2\pi\sqrt{\kappa}\,X)) \approx \frac{16\pi^3\kappa^{3/2}l^3(3+2\pi^2\kappa l^2)}{\sinh(\pi^2\sqrt{\kappa}\,l)}\sin(2\pi\sqrt{\kappa}\,X), \tag{A8}$$

$$\begin{aligned} I_9 &= -\pi^2\sqrt{\kappa}\,l - \sum_{n=1}^{\infty}\frac{\pi^2\sqrt{\kappa}\,l}{2\sinh^4(n\pi^2\sqrt{\kappa}\,l)}\Big[(-6+23n^2\pi^4\kappa\,l^2)\cosh(n\pi^2\sqrt{\kappa}\,l)+(6+n^2\pi^4\kappa\,l^2)\cosh(3n\pi^2\sqrt{\kappa}\,l) \\ &\quad -6n\pi^2\sqrt{\kappa}\,l\Big(5\sinh(n\pi^2\sqrt{\kappa}\,l)+\sinh(3n\pi^2\sqrt{\kappa}\,l)\Big)\Big]\cos(2n\pi\sqrt{\kappa}X) \approx -\pi^2\sqrt{\kappa}\,l, \end{aligned} \tag{A9}$$

$$\begin{aligned} I_{10} &= \frac{2}{3}\pi^2\sqrt{\kappa}\,l - \sum_{n=1}^{\infty}\frac{\pi^2\sqrt{\kappa}\,l}{\sinh^3(n\pi^2\sqrt{\kappa}\,l)}\Big[2n\pi^2\sqrt{\kappa}\,l\Big(3+\cosh(2n\pi^2\sqrt{\kappa}\,l)\Big)-4\sinh(2n\pi^2\sqrt{\kappa}\,l)\Big]\cos(2n\pi\sqrt{\kappa}X) \\ &\approx \frac{2}{3}\pi^2\sqrt{\kappa}\,l, \end{aligned} \tag{A10}$$

$$I_{11} = -2\pi^2\sqrt{\kappa}\,l\sum_{n=1}^{\infty}\frac{\tanh(n\pi^2\sqrt{\kappa}\,l)}{\cosh(n\pi^2\sqrt{\kappa}\,l)}\sin(2\pi\sqrt{\kappa}\,X) \approx -\frac{2\pi^2\kappa^{1/2}l\tanh(\pi^2\sqrt{\kappa}\,l)}{\cosh(\pi^2\sqrt{\kappa}\,l)}\sin(2\pi\sqrt{\kappa}\,X), \tag{A11}$$

$$\begin{aligned} I_{12} &= I_{11} + \sum_{n=1}^{\infty}\frac{2\pi\sqrt{\kappa}\,l}{3\cosh(n\pi^2\sqrt{\kappa}\,l)}\Big[(3\pi+8n^2\pi^3\kappa\,l^2-16n^4\pi^5\kappa^2\,l^4)\tanh(n\pi^2\sqrt{\kappa}\,l)+16n\pi\sqrt{\kappa}\,l(4n^2\pi^2\kappa\,l^2-1)\Big] \\ &\quad \times\sin(2n\pi\sqrt{\kappa}X) \approx \frac{16\pi^2\kappa l^2}{3\cosh(\pi^2\sqrt{\kappa}\,l)}\Big[-2+8\pi^2\kappa l^2+\pi^2\sqrt{\kappa}\,l(1-2\pi^2\kappa\,l)\tanh(\pi^2\sqrt{\kappa}\,l)\Big]\sin(2\pi\sqrt{\kappa}\,X), \end{aligned} \tag{A12}$$

$$\begin{aligned} I_{13} &= I_2 - 8\sqrt{\kappa}\,l - \sum_{n=1}^{\infty}\frac{16n\pi^2\kappa\,l^2}{\sinh(n\pi^2\sqrt{\kappa}\,l)}\Big[2(1+2n^2\pi^2\kappa\,l^2)-n\pi^2\sqrt{\kappa}\,l(1+n^2\pi^2\kappa\,l^2)\coth(n\pi^2\sqrt{\kappa}\,l)\Big]\cos(2n\pi\sqrt{\kappa}X) \\ &\approx -12\sqrt{\kappa}\,l. \end{aligned} \tag{A13}$$

Clearly, since $l(t)$ is an oscillating function around $l_0 \approx 1$, the sums $I_2, I_4, I_6, I_9, I_{10}$ and I_{13} are $\mathcal{O}(\kappa^{1/2})$. In Fig. 8, we have plotted the amplitudes of the remaining series, I_8, I_7, I_3, I_1, I_5, I_{11} and I_{12} from top to bottom, versus the coupling parameter κ in order to weigh up the importance of each term in Eqs.(19) and (20). These amplitudes have been evaluated at $l(t) \approx 1$ due to the small size of the fluctuations of the kink width. From Fig. 7, it is clear that I_5, I_{11} and I_{12} are much smaller than the rest and can be dropped in Eqs. (19)-(20).

Acknowledgments

N.R.Q. acknowledges financial support through grant FIS2011-24540 from the Ministerio de Economía y Competitividad (Spain), grants FQM207, P09-FQM-4643 from Junta de Andalucía (Spain), and a grant from the Humboldt Foundation through a Research Fellowship for Experienced Researchers SPA 1146358 STP.

[1] F. Marchesoni, Phys. Rev. Lett. **77**, 2364 (1996).

[2] M. Salerno and N. R. Quintero, Phys. Rev. E, **65** 025602(R)

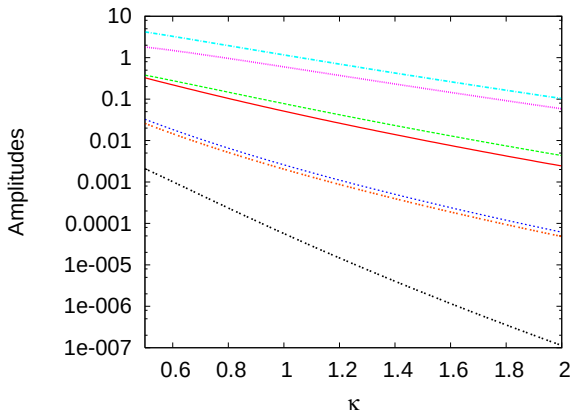

FIG. 8: (Color online) Amplitudes of the series I_8, I_7, I_3, I_1, I_5, I_{11} and I_{12} (from top to bottom) versus coupling. The amplitudes have been evaluated at $l(t) \approx 1$ due to the small size of the fluctuations of $l(t)$.

(2002).
[3] G. Costantini, F. Marchesoni and M. Borromeo, Phys. Rev. E **65**, 051103 (2002).
[4] P. Reimann Phys. Rep. **361**, 57 (2002); P. Hänggi and R. Bartussek, in *Lecture notes in Physics*, Ed.s J. Parisi et al., Springer, Berlin, **476** (1996).
[5] M. Salerno and Y. Zolotaryuk. Phys. Rev. E **65**, 056603 (2002).
[6] S. Flach, Y. Zolotaryuk, A. E. Miroshnichenko, and M. V. Fistul. Phys. Rev. Lett. **88**, 184101 (2002).
[7] G. Carapella and G. Costabile, Phys. Rev. Lett. **87**, 077002 (2001); G. Carapella, Phys. Rev. B **63**, 054515 (2001).
[8] M. Beck, E. Goldobin, M. Neuhaus, M. Siegel, R. Kleiner and D. Koelle, Phys. Rev. Lett. **95**, 090603 (2005).
[9] E. Trías, J.J. Mazo, F. Falo and T.P. Orlando, Phys. Rev. E **61**, 2257 (2000).
[10] D.E. Shalom and H. Pastoriza, Phys. Rev. Lett. **94**, 177001 (2005).
[11] A. V. Ustinov, C. Coqui, A. Kemp, Y. Zolotaryuk and M. Salerno, Phys. Rev. Lett. **93**, 087001 (2004).
[12] L. Morales-Molina,N. R. Quintero, F. G. Mertens and A. Sánchez, Phys. Rev. Lett. **91**, 234102 (2003).
[13] N. R. Quintero, B. Sánchez-Rey and M. Salerno, Phys. Rev. E **72**, 016610 (2005); N. R. Quintero, R. Alvarez-Nordase and F. G. Mertens, Phys. Rev. E **80**, 016605 (2009).
[14] L. Morales-Molina, F. G. Mertens and A. Sánchez, Eur. Phys. J. B **3**7, 79 (2004).
[15] L. Morales-Molina, F. G. Mertens and A. Sánchez, Phys. Rev. E **7**2, 016612 (2005).
[16] Y. Zolotaryuk and M. Salerno Phys. Rev. E **73**, 066621 (2006).
[17] J. Cuevas, B. Sánchez-Rey and M. Salerno, Phys. Rev. E **82**, 016604 (2010).
[18] A. Gorbach, S. Denisov and S. Flach, Opt. Lett. **31**, 1702 (2006).
[19] P.J. Martínez and R. Chacon, Phys. Rev. Lett. **100**, 144101 (2008).
[20] Y. Yang, et. al., Eur. Phys. Lett. **93**, 16001 (2001).
[21] Y. Zolotaryuk, Phys. Rev. E **86**, 026604 (2012).
[22] Oleg M. Braun and Yuri S. Kivshar, Phys. Rep. **306**, 2 (1998).
[23] Oleg M. Braun and Yuri S. Kivshar, *The Frenkel-Kontorova Model: Concepts, Methods and Applications*, Springer-Verlag, Berlin-Heidelberg, 2004.
[24] J. Cuevas-Maraver, P.G. Kevrekidis, and F. Williams, eds. *The sine-Gordon Model and its Applications. From Pendula and Josephson Junctions to Gravity and High Energy Physics*, Springer-Verlag, Berlin-Heidelberg. In press.
[25] F. Falo, P.J. Martínez, J.J. Mazo and S. Cilla, Europhys. Lett. **45**, 700 (1999)
[26] A. V. Ustinov, M. Cirillo and B. Malomed, Phys. Rev. B **47**, 8357 (1993).
[27] M. Salerno, Physica **D17**, 227 (1985).
[28] M.J. Rice and E.J. Mele, Solid State Commun. **35**, 487 (1980); M. Salerno and A.C. Scott Phys. Rev. B **26**, 2474 (1982).
[29] L. A. Cisneros and A. A. Minzoni, Physica D **237**, 50 (2008).
[30] A. V. Ustinov, T. Doderer, R.P. Huebener, N.F. Pedersen, B. Mayer and U.A. Oboznov, Phys. Rev. Lett. **69**, 1815 (1992).
[31] F.G. Mertens, H.J. Schnitzer and A. R. Bishop, Phys. Rev. B, **56**, 2510 (1997).
[32] T. Kamppeter et al., Phys. Rev. B, **59**, 11349 (1999); T. Kamppeter et al., Eur. Phys. J. B, **7**, 607 (1999).
[33] N.R. Quintero, A. Sánchez and F.G. Mertens, Phys. Rev. E, **62**, 5695 (2000).
[34] N. R. Quintero, J.A. Cuesta and R. Álvarez-Nodarse, Phys. Rev. E, **81**, 030102 (2010).
[35] J.A. Cuesta, N. R. Quintero and R. Álvarez-Nodarse, Phys. Rev. X **3**, 041014 (2013).
[36] J.L. Marín, F. Falo, P.J. Martínez and L.M. Floría, Phys. Rev. E **63**, 066603 (2001).
[37] L.M. Floría and J. J. Mazo, Adv. Phys. **45**, 505 (1996).
[38] N.R. Quintero, J.A. Cuesta and R. Álvarez-Nodarse, J. Phys. A: Math. Theor. **44**, 425205 (2011).